Mouse genetics reveals Barttin as a genetic modifier of Joubert syndrome

Simon A. Ramsbottom[a], Peter E. Thelwall[a,b], Katrina M. Wood[c], Gavin J. Clowry[d], Laura A. Devlin[a], Flora Silbermann[e], Helena L. Spiewak[f], Shirlee Shril[g], Elisa Molinari[a], Friedhelm Hildebrandt[g], Meral Gunay-Aygun[h,i,j], Sophie Saunier[e], Heather J. Cordell[k], John A. Sayer[a,d,l,1], and Colin G. Miles[a,1]

[a]Translational and Clinical Research Institute, Faculty of Medical Sciences, Newcastle upon Tyne NE1 3BZ, United Kingdom; [b]Newcastle Magnetic Resonance Centre, Newcastle University, Newcastle upon Tyne NE4 5PL, United Kingdom; [c]The Histopathology Department, The Newcastle upon Tyne Hospitals National Health Service (NHS) Foundation Trust, Newcastle upon Tyne NE7 7DN, United Kingdom; [d]Biosciences Institute, Faculty of Medical Sciences, Newcastle University, Newcastle upon Tyne NE2 4HH, United Kingdom; [e]Laboratory of Hereditary Kidney Disease, Imagine Institute, INSERM U1163, Université de Paris, 75015 Paris, France; [f]Northern Genetics Service, International Centre for Life, The Newcastle upon Tyne Hospitals NHS Foundation Trust, Newcastle upon Tyne NE1 3BZ, United Kingdom; [g]Division of Nephrology, Department of Medicine, Boston Children's Hospital, Harvard Medical School, Boston, MA 02115; [h]Medical Genetics Branch, National Human Genome Research Institute, National Institutes of Health, Bethesda, MD 20892; [i]Department of Pediatrics, Johns Hopkins University School of Medicine, Baltimore, MD 21287; [j]McKusick-Nathans Institute of Genetic Medicine, Johns Hopkins University School of Medicine, Baltimore, MD 21287; [k]Population Health Sciences Institute, Faculty of Medical Sciences, Newcastle University, Newcastle upon Tyne NE1 3BZ, United Kingdom; and [l]National Institute for Health Research Newcastle Biomedical Research Centre, Newcastle upon Tyne NE4 5PL, United Kingdom

Genetic and phenotypic heterogeneity and the lack of sufficiently large patient cohorts pose a significant challenge to understanding genetic associations in rare disease. Here we identify *Bsnd* (alias *Barttin*) as a genetic modifier of cystic kidney disease in Joubert syndrome, using a *Cep290*-deficient mouse model to recapitulate the phenotypic variability observed in patients by mixing genetic backgrounds in a controlled manner and performing genome-wide analysis of these mice. Experimental down-regulation of *Bsnd* in the parental mouse strain phenocopied the severe cystic kidney phenotype. A common polymorphism within human *BSND* significantly associates with kidney disease severity in a patient cohort with *CEP290* mutations. The striking phenotypic modifications we describe are a timely reminder of the value of mouse models and highlight the significant contribution of genetic background. Furthermore, if appropriately managed, this can be exploited as a powerful tool to elucidate mechanisms underlying human disease heterogeneity.

ciliopathy | genetics | modifier | Joubert syndrome | Barttin

Rare disease represents a healthcare burden estimated to affect ~350 million people worldwide (1). Phenotypic variability is a confounding factor in understanding genetic disease and often results from the underlying background genetics. The concept of modifying genes that have little or no effect on a phenotype in isolation but can alter the phenotype of a particular mutation was recognized a century ago in *Drosophila* (2) and subsequently shown to be an important factor in human disease (3). While the identification of modifying genes has been simplified by developments in genome-wide analyses and the availability of increasingly large patient cohorts (4, 5), genetic modifiers in rare disease remain inherently intractable due to the scarcity of patients.

Defects of the primary cilium result in a number of syndromes, collectively known as ciliopathies, that exemplify the challenges faced when attempting to understand genotype–phenotype heterogeneity in rare disease (6–8). Joubert syndrome is regarded as the archetypal ciliopathy, with one of the most common causes being biallelic mutations in the *CEP290* gene (9, 10). However, mutations in *CEP290* can result in a phenotypic spectrum (11–17) ranging from retinal degeneration alone (Leber congenital amaurosis) to embryonic lethality (Meckel–Gruber syndrome). In many cases, phenotypic variability is evident among patients harboring identical mutations, with no clear genotype–phenotype correlations.

Recently, the mouse has been shown to provide a good model for numerous ciliopathies and these models have begun to elucidate the underlying mechanisms of these diseases (18–21). Furthermore, there is evidence to suggest that murine ciliopathy phenotypes are influenced by genetic modifiers. The $Cep290^{Gt(CC0582)Wtsi}$ mouse, for example, which presents with retinal degeneration, slowly progressing cystic kidney disease, and hydrocephalus on a 129/Ola genetic background, is embryonic lethal on a C57BL/6 background and shows a variable phenotype ranging from embryonic lethality to severe cystic kidney disease on a 129/Sv genetic background (19). This heterogeneity is indicative of the presence of strain-specific genetic modifiers of the phenotype and is consistent with the heterogeneity seen in *CEP290* ciliopathy patients.

Results and Discussion

In order to identify potential loci modifying murine Joubert syndrome and establish whether mouse genetics could provide a convenient way of identifying modifier genes in rare human diseases more generally, we intercrossed $Cep290^{Gt(CC0582)Wtsi}$ mice

Significance

Our current understanding of genetic disease is often inadequate, largely due to genetic background effects that modify disease presentation. This is particularly challenging for rare diseases that lack sufficient numbers of patients for genome-wide association studies. We show in a series of experiments using a murine model of Joubert syndrome, a multisystem ciliopathy, that a single locus is a modifier of cystic kidney disease. We go on to show that the human homolog plays a similar role in disease using a cohort of patients. These findings make a significant contribution to the underplayed (and often ignored) role of genetic background in murine models and how this can be exploited to understand further rare inherited disease.

GENETICS

(a hypomorphic allele, MGI:3870362; hereafter referred to as *Cep290*[Gt] mice) to mix their genetic background in a controlled manner (Fig. 1*A*). Heterozygous *Cep290*[Gt] first generation (F1) (129/Ola x C57BL/6) animals were bred to generate homozygous *Cep290*[Gt/Gt] F2 mice that were analyzed at 3 wk of age. The number of homozygous mutant mice recovered from these crosses deviated significantly from the expected Mendelian ratio (χ^2, $P < 0.005$), suggesting that ~40% of homozygous animals died in utero, consistent with previous reports (22, 23). Viable homozygous animals tended to be smaller than littermates (6.6 vs. 11.6 g at postnatal day 21; *SI Appendix*, Fig. S1*B*), displaying varying degrees of cranial doming, a feature associated with hydrocephalus (*SI Appendix*, Fig. S1*A*).

Retinal abnormalities were observed in homozygous *Cep290*[Gt/Gt] F2 mice, similar to the phenotype previously described for the inbred (129/Ola) strain (19), with complete loss of the outer segment of the photoreceptor layer in all homozygous mutant animals (*SI Appendix*, Fig. S1*C*). This suggests that the photoreceptor phenotype is not affected by genetic modifiers, given that it is severe in both the genetic backgrounds we have studied. Variability in the extent of cell loss within the outer and inner nuclear and plexiform layers was observed but showed no consistent trends across the cohort, and association analyses

revealed no genetic associations (*SI Appendix*, Fig. S2 *E* and *F*). It should be noted that at the time point of phenotyping (P21), retinal development is ongoing and therefore the observed variability may be in part due to differences in rates of development.

Homozygous F2 *Cep290*[Gt/Gt] mice displayed hydrocephalus, as previously reported for the inbred (129/Ola) strain (19). However, high-resolution ex vivo MRI (in a subset of animals) revealed structural defects within the cerebellum (Fig. 1 *B* and *C* and *SI Appendix*, Fig. S1*D*) that are not found in mutant mice on a 129/Ola genetic background, indicating that the phenotype of the *Cep290*[Gt/Gt] Joubert syndrome mouse can be modified to include cerebellar aplasia phenotypes typical of patients by alteration of the genetic background. Cerebellar lobule-specific defects observed include hypoplasia of the folium–tuber vermis (lobule VII) and pyramus (VIII), with some mice also displaying additional degeneration within the uvula (IX) and nodulus (X). It is noteworthy that mutant mice with structural abnormalities of the nodulus (X), which forms part of the vestibulocerebellum and is crucial for maintaining balance, displayed overt symptoms of ataxia, a common feature of Joubert syndrome patients (10, 24, 25). It should be noted that the presence of foliation defects did not correlate with the degree of hydrocephalus, suggesting that additional, tissue-specific, phenotypic modifiers exist.
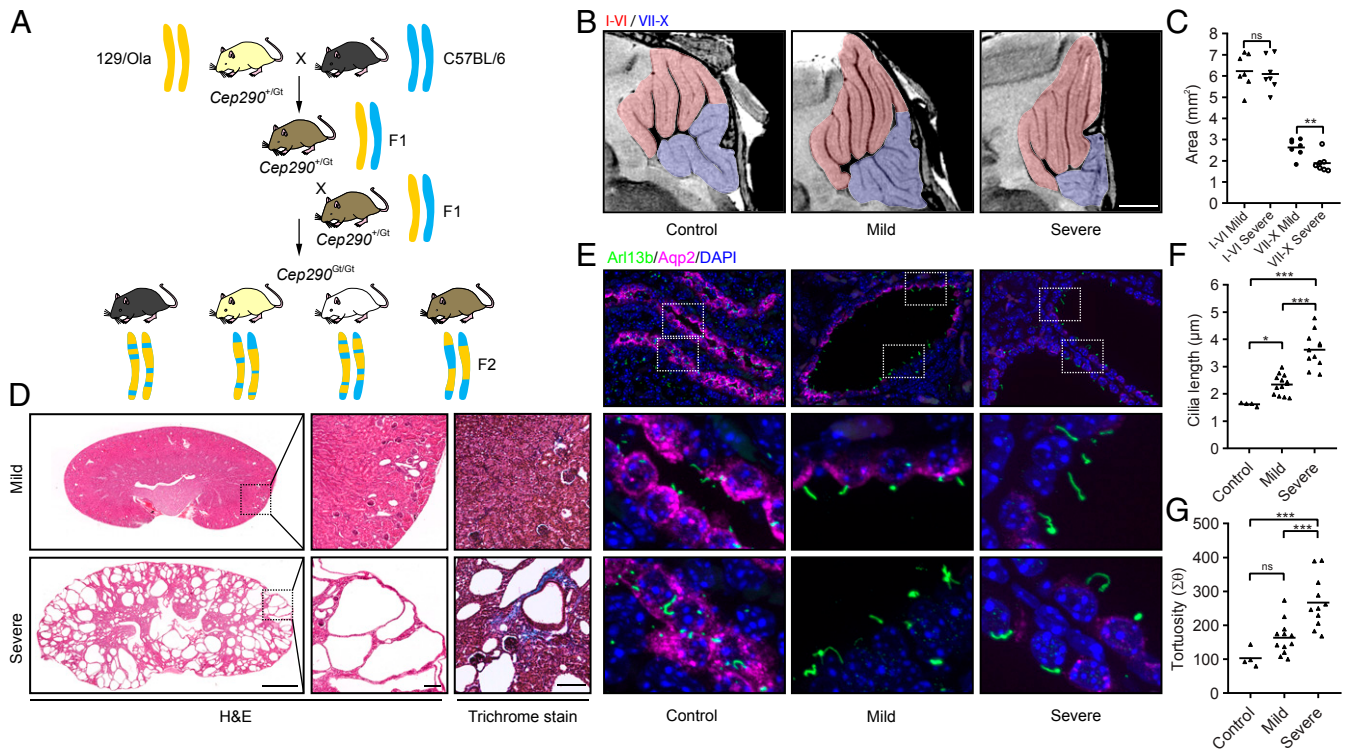
Fig. 1. Phenotypic spectrum of an F2 *Cep290*[Gt/Gt] mouse model of Joubert syndrome. (*A*) Schematic showing mouse breeding strategy. *Cep290*[Gt/+] heterozygous mice on a 129/Ola background were bred with wild-type C57BL/6 mice to generate F1 hybrids. F1 *Cep290*[Gt/+] heterozygous mice were then interbred to give F2 *Cep290*[Gt/Gt] homozygous animals with a randomized set of alleles from both parent strains. Representative alleles from 129/Ola and C57BL/6 mice are shown in yellow and blue, respectively. Variable coat colors in F2 mice from this cross are shown including black, chinchilla, albino, and agouti (*Left* to *Right*). (*B*) High-resolution ex vivo MRI showing morphologically aberrant cerebellar structures in P21 F2 *Cep290*[Gt/Gt] mice. A subset of F2 *Cep290*[Gt/Gt] mice shows localized aplasia within the cerebellum, specifically within the folium–tuber vermis, pyramus, uvula, and nodulus (lobules VII to X, respectively; blue overlay). Lobules I to VI appear largely unaffected (red overlay); flattening of the cerebellum against the skull can be observed in all *Cep290*[Gt/Gt] animals as a result of hydrocephalus. Representative images of wild-type control, mild, and severe animals are shown. (Scale bar, 1 mm.) (*C*) Quantification of the sagittal cross-sectional area of lobules I to VI compared with VII to X of the cerebellum in mild and severe F2 *Cep290*[Gt/Gt] animals (Student's *t* test, **P < 0.01; ns, not significant). (*D*) Hematoxylin and eosin (H&E) and Masson's Trichrome images of kidneys from F2 *Cep290*[Gt/Gt] mice showing a large degree of phenotypic heterogeneity in terms of the number and size of cysts, as well as the amount of interstitial fibrosis as indicated by increased collagen deposition (blue staining). (Scale bars, 1 mm [main images] and 100 μm [expanded views].) (*E*) Immunofluorescence staining of P21 mouse kidney from F2 *Cep290*^{+/+} and *Cep290*[Gt/Gt] animals, showing the expression of the ciliary GTPase Arl13b (green) and the water channel Aquaporin 2 (Aqp2; magenta). The 2 *Lower* in each column are magnified regions from the *Upper* identified by dotted boxes. (Scale bars, 10 μm.) (*F* and *G*) Quantification of cilia length (*F*) and tortuosity (*G*) in F2 *Cep290*^{+/+} and *Cep290*[Gt/Gt] animals (1-way ANOVA, *P < 0.05, **P < 0.01, ***P < 0.001).

While the majority of homozygous mutant kidneys appeared grossly normal, several were pale and enlarged, resembling the kidney previously reported from a *Cep290*^{Gt/Gt} mouse bred on a mixed C57BL/6J-129/SvJ background (23). Renal histopathology revealed a striking variability in cystic burden ranging in severity from a few small cysts to multiple large cysts with early stages of fibrosis and collagen deposition typical of nephronophthisis (Fig. 1*D* and *SI Appendix*, Fig. S1*E*). In order to avoid bias, cystic burden was quantified in an automated way to give a "cystic index" value that enabled the severity of kidney disease to be ranked from 0 to 52%, with the majority of animals ($n = 66$) falling in the 0 to 5% range (*SI Appendix*, Figs. S1*F* and S4). There was no correlation between cystic index of the kidneys and retinal layer loss (*SI Appendix*, Fig. S1*G*), while the most severe cerebellar disease was associated with severe cystic kidney disease (*SI Appendix*, Fig. S1*H*).

CEP290, a transition-zone protein, has been shown to be required for normal cilia morphology in both human and mouse (19, 26–28). Immunofluorescence staining for Arl13b, a GTPase which is spatially restricted to the ciliary membrane, revealed elongated primary cilia in all F2 homozygous mutant kidneys compared with wild-type littermates (Fig. 1 *E* and *F*). Costaining with Aquaporin 2 (Aqp2), a water channel found at the apical surface of principal cells of the collecting duct, revealed that cysts containing elongated cilia were found predominantly in the distal part of the nephron (Fig. 1*E*). Kidneys with the highest cystic index, however, presented with significantly longer cilia than those with a low cystic index, and a strong association was observed between cilia length and average cyst size ($R^2 = 0.82$, $P < 0.0001$; *SI Appendix*, Fig. S1*I*). Cilia from kidneys with a high cystic index also displayed increased tortuosity (Fig. 1 *E* and *G* and *SI Appendix*, Fig. S1*J*), consistent with the elongated, tortuous cilia seen in Joubert syndrome patient renal biopsies (28). Furthermore, epithelial cells of the collecting duct showed an almost complete loss of Aqp2 expression from the apical surface in kidneys from the most severely affected animals (Fig. 1*E*).

Given that our cohort of F2 mutant mice presented with a range of phenotypes consistent with the presence of strain-specific modifier loci, we designed a panel of 932 informative single-nucleotide polymorphisms (SNPs; of which 789 subsequently passed quality control) across the genome (*SI Appendix*, Fig. S2*A*) to distinguish between 129/Ola and C57BL/6 strains to allow identification of potential modifiers. Seventy-seven mice were genotyped in this way with a call rate of 96.3% (at an average resolution of 2 to 3 Mb). The average number of recombination events across the population of homozygous *Cep290*^{Gt/Gt} mice was 39, which was invariant across the cystic kidney phenotypic range (*SI Appendix*, Fig. S2 *C* and *D*). The approach was first validated using coat color as a variable trait. As predicted, strong associations were identified in mice with black coat color (homozygosity for the *nonagouti* locus) on chromosome 2 (Fig. 2 *A* and *B*) and mice with albino/chinchilla coat color (homozygosity for the *tyrosinase* locus) on chromosome 7 (Fig. 2 *C* and *D*), thus confirming that our experimental approach was capable of identifying known genetic associations.

Similar to Joubert syndrome patients, the most striking phenotypic heterogeneity in our mouse cohort was the severity of kidney disease. We therefore sought to identify a modifier locus associated with an increased potential of developing cystic kidney disease in our *Cep290*^{Gt/Gt} mice. Using the cystic index of the kidneys as a continuous variable trait with a recessive pattern of inheritance, a strong association with a single locus on chromosome 4, delineated by rs3664701 and rs3659850, was identified (Fig. 2 *E* and *F* and *SI Appendix*, Fig. S2*B*). All mice with a severe kidney phenotype (11 animals with cystic index >10%; Fig. 2) were homozygous for SNPs inherited from the C57BL/6 background. A single mouse homozygous for C57BL/6 fell below the 10% threshold but was ranked the next most severe with a cystic

index of 7.1%, whereas all other mice were either homozygous or heterozygous for 129/Ola–inherited SNPs and displayed a mild kidney phenotype (65 animals). The size of this locus is 5.075 Mb and corresponds to ~0.18% of the mouse genome. The deviation from Hardy–Weinberg equilibrium was determined for each locus across the genome (Fig. 2 *G* and *H*), revealing that only the *Cep290* locus on mouse chromosome 10 showed any deviation. This is to be expected, as all mice were selected as homozygous for the *Cep290* mutation that was initially introduced into 129/Ola mouse embryonic stem cells (19).

Having identified a locus modifying the severity of kidney disease in murine Joubert syndrome, we went on to investigate loci associated with the severity of renal disease in Joubert syndrome patients. Initially, a cohort of 6 patients was assembled, 3 with early-onset end-stage renal disease (ESRD) and 3 with mild/no renal involvement, selected on the basis of having identical causative mutations in *CEP290* [homozygous c.5668G>T; p.(Gly1890*)]. A whole exome-wide search of variants segregating with disease severity in these patients revealed over 300 potential modifier loci associating with kidney disease. However, selecting only loci within the region syntenic to the mouse modifier locus (human chromosome 1p32) resulted in SNPs associated with severe kidney disease in Joubert syndrome patients linked to just 2 adjacent genes—*BSND* (rs2500341) and *TMEM61* (rs2253466) (Table 1).

TMEM61 is reported to be expressed in a tissue-specific manner, with the highest RNA levels in glandular tissues such as endocrine (parathyroid), salivary, and seminal vesicle, with lower levels found in kidney; however, there are insufficient data to reliably annotate protein expression in human (https://www.proteinatlas.org/ENSG00000143001-TMEM61/tissue), while mouse *Tmem61* is annotated as a lincRNA.

BSND encodes Barttin, a subunit of the chloride channels CLCNKA and CLCNKB, essential for renal salt reabsorption that has previously been shown to cause Bartter syndrome with sensorineural deafness (29). In mouse kidney, *Bsnd* is expressed in the thin limb and the thick ascending limb of the loop of Henle (29) and intercalated cells of the cortical collecting duct (30) (*SI Appendix*, Fig. S3*A*). Of note, Barttin expression is found in small cysts of homozygous F2 mutant mice but appears to be lost in large cysts (*SI Appendix*, Fig. S3*A*). Bartter syndrome patients with *BSND* mutations have reduced urine-concentrating capacity, resulting in increased urine production (polyuria) and chronic kidney disease which may progress to ESRD (31, 32), as do Joubert syndrome patients with renal involvement (nephronophthisis) (33, 34). It is noteworthy that the mutations in *CFTR* encoding an apical chloride channel may also modify cystic kidney disease phenotypes in patients with autosomal dominant polycystic kidney disease, highlighting the importance of chloride transport in cyst expansion (35).

rs2500341 is located within the 5′ UTR of *BSND* and the variant associated with severity of kidney disease (G) has a frequency of 0.595 within 1000 Genomes (global) (https://www.internationalgenome.org) but is markedly more prevalent in European (G = 0.759) and American (G = 0.70) populations. In addition, rs2500341 is annotated as an eQTL, with the G allele linked with lower levels of *BSND* expression within the brain (https://gtexportal.org/home/). Coupled with the reduced expression observed in the most severely affected mouse kidneys, we hypothesized that lower expression of *Bsnd* from the C57BL/6 locus could be responsible for increased cystic disease. To test this hypothesis, we sought to determine the consequences of reducing *Bsnd* expression in pure, inbred 129/Ola homozygous mutant *Cep290*^{Gt/Gt} mice (Fig. 3*A*). Systemic administration, via tail vein injection, of a *Bsnd* antisense oligonucleotide (ASO) targeting the translational start site over 12 d resulted in a significant reduction in Bsnd protein levels within the kidney (Fig. 3*B* and *SI Appendix*, Figs. S3*C* and S5*A*). Immunohistochemical analysis revealed loss of Aquaporin 2 in principal cells of the cortical collecting duct and primary cilia with increased tortuosity, compared with control

GENETICS

www.manaraa.com
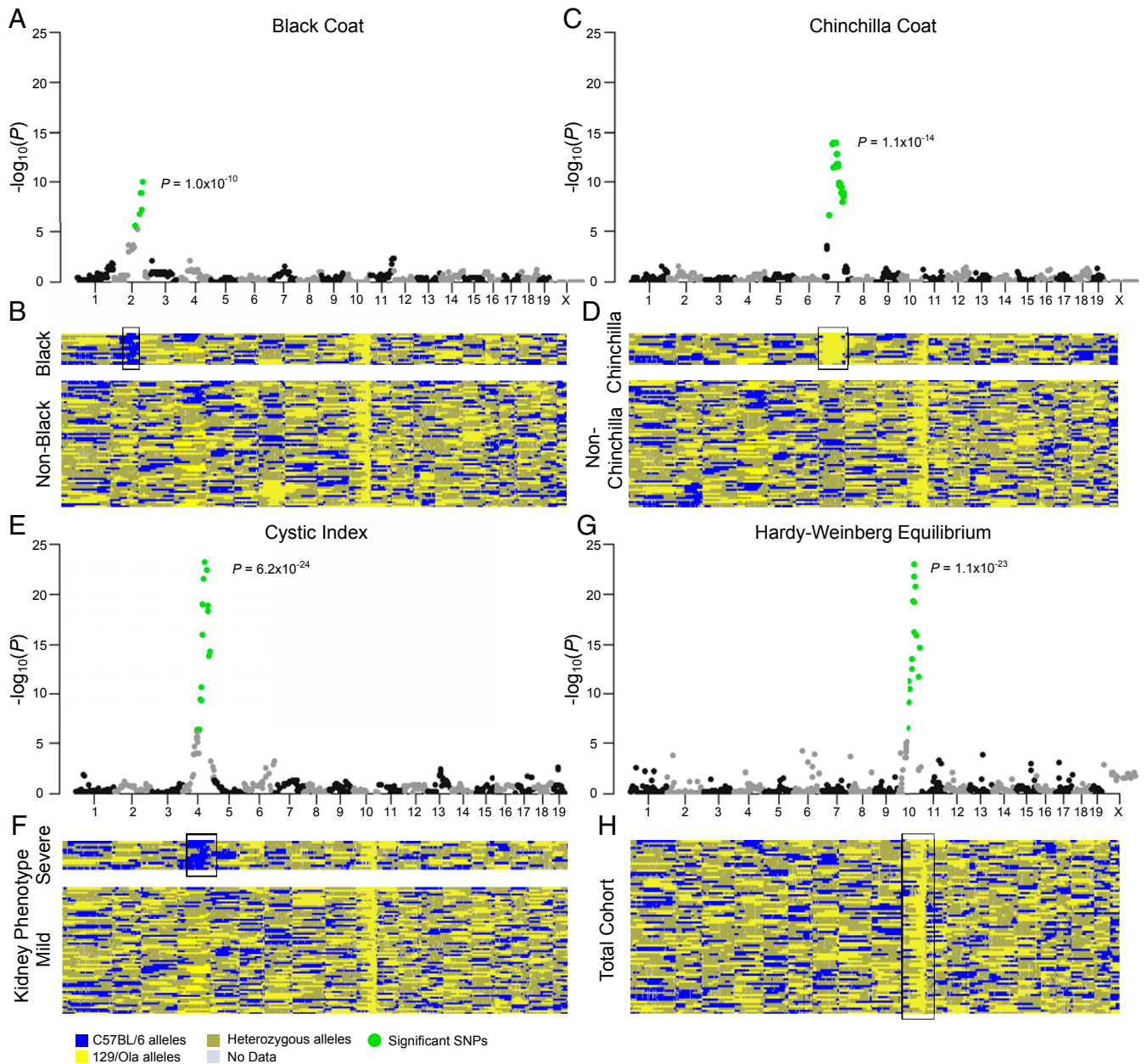
Fig. 2. Modifier locus in chromosome 4 affects the kidney phenotype in F2 *Cep290*^Gt/Gt mice. (*A*, *C*, and *E*) Manhattan plots showing the strength of association of each variant with coat color (*A* and *C*) or severe kidney disease (*E*) ordered according to genomic position. Significant SNPs are shown in green ($P < 6.34 \times 10^{-5}$). (*B*, *D*, and *F*) Genotyping heatmaps showing alleles inherited from either the C57BL/6 strain (blue) or the 129/Ola strain (yellow). Heterozygous calls are shown in gold. Reads lacking data are shown in gray. Samples are shown *Top* to *Bottom* in order of coat color (*B* and *D*) or cystic index (*F*). Mice displaying the phenotype of interest for each plot are shown (*Upper*) (*B*, black coat; *D*, chinchilla coat; *F*, severe kidney phenotype, cystic index > 10%). (*G*) Manhattan plot showing the deviation from the Hardy–Weinberg equilibrium at each locus ordered according to genomic position. The only significant SNPs are located adjacent to the locus of *Cep290*. (*H*) Genotyping heatmap showing alleles inherited from either parent strain. All mice are shown in a randomized order. The position of significant SNPs is identified in each heatmap (black bounding box). For each plot, the *P* value of the most significant SNP is shown.

129/Ola *Cep290*^Gt kidneys (Fig. 3 *C* and *D*). Injection of *Bsnd* ASO in wild-type 129/Ola mice did not produce any ciliary phenotype (*SI Appendix*, Fig. S5B), consistent with the concept of a genetic modification that has little or no phenotypic effect in isolation. These data indicate that reduction of Bsnd within kidneys of pure 129/Ola *Cep290*^Gt/Gt mutant mice phenocopies the severe F2 mice that are homozygous for C57BL/6–derived *Bsnd*. Furthermore, immunohistochemical analysis of a Joubert syndrome patient (NPH621: G/G at rs2500341; *SI Appendix*, Table S1) kidney biopsy at ESRD reveals a remarkably similar phenotype to the mouse models (both *Bsnd* knockdown in 129/Ola and severe F2 mutant

Cep290^Gt/Gt), including loss of Aquaporin 2 expression and elongated, tortuous primary cilia (Fig. 3*E*). A reduction of Barttin expression in epithelial cells lining the cysts in kidney tissue from patient NPH621 can also be seen (*SI Appendix*, Fig. S3B), consistent with the findings observed in F2 *Cep290*^Gt/Gt mice.

Having identified *Bsnd* as a modifier gene for the renal manifestation of murine Joubert syndrome and observed confirmatory evidence in a patient biopsy, we extended our analysis in humans to assess the relevance of this finding in a wider cohort of *CEP290* ciliopathy patients with variable phenotypes (*SI Appendix*, Table S1). Patients were defined as having a high severity

www.manaraa.com

Table 1. Common SNPs in *BSND* and *TMEM61* are associated with increased kidney involvement in Joubert syndrome patients with *CEP290* mutations

Sample	*CEP290* mutation 1	*CEP290* mutation 2	Kidney phenotype	Kidney disease score[†]	rs2500341 MAF (C) 0.24	rs2253466 MAF (C) 0.39
F394	c.5668G>T; p.(Gly1890*)	c.5668G>T; p.(Gly1890*)	Enlarged cystic kidneys ESRD age 12 y	High	GG	TT
F700	c.5668G>T; p.(Gly1890*)	c.5668G>T; p.(Gly1890*)	Bilateral small hyperechogenic kidneys ESRD age 11 y	High	GG	TT
F944	c.5668G>T; p.(Gly1890*)	c.5668G>T; p.(Gly1890*)	Bilateral small hyperechogenic kidneys ESRD age 13 y	High	GG	TT
B1106	c.5668G>T; p.(Gly1890*)	c.5668G>T; p.(Gly1890*)	Hyperechogenic kidneys CKD stage 2, age 10 y	Low	CG	CT
F02	c.5668G>T; p.(Gly1890*)	c.5668G>T; p.(Gly1890*)	Hyperechogenic kidneys CKD stage 1, age 15 y	Low	CG	CT
A1188	c.5668G>T; p.(Gly1890*)	c.5668G>T; p.(Gly1890*)	Hyperechogenic kidneys CKD stage 1, age 11 y	Low	CG	CT

[†]Patients were scored based on their level of kidney function and the presence of cysts in the kidneys as shown by renal ultrasound scanning. A high disease score indicates limited or no residual kidney function and/or the presence of multiple cysts within the kidney. CKD, chronic kidney disease; ESRD, end-stage renal disease; MAF, minor allele frequency. Genotype is denoted as GG, TT, CG, or CT; where G is guanine, T is thymine, and C is cytosine.

score of kidney disease if they had either progressed to ESRD or were shown to have multiple cysts within their kidneys. In all 11 *CEP290* ciliopathy patients with absent/mild kidney disease phenotypes, we did not observe the "severe" (G/G) *BSND* haplotype at rs2500341, whereas 12/18 patients with severe kidney disease phenotypes were homozygous for this common variant (Fisher's

exact test, $n = 29$, $P = 0.00002$), indicating a significant association between rs2500341 and severity of kidney disease phenotype.

This study describes the first steps toward elucidating the seemingly intractable phenotypic heterogeneity observed in ciliopathy patients and, while the association we have revealed is not 100% discriminatory for kidney disease severity in Joubert syndrome, it lays the foundations for increasing our understanding of the heterogeneity of ciliopathies. We have revealed patient phenotypes at the cellular level in unprecedented detail, and confirmed the importance of mouse models, highlighting the need for consideration of genetic background effects. Furthermore, we have demonstrated that with the a priori knowledge afforded by mouse genetics, it is possible to discover genetic association in rare diseases within small cohorts of patients.

The striking phenotypic modifications observed in our F2 animals serve as a timely reminder of the value of mouse models but also of the potentially confounding effects resulting from genetic background. If appropriately managed, however, these effects can be exploited, providing a powerful tool to approach human disease heterogeneity.

Materials and Methods

Further information can be found in *SI Appendix*, Figs. S1–S6, and Table S1.

Statistics. All individual tests of numerical data were performed using an unpaired Student's t test or a 1-way ANOVA followed by a Bonferroni-corrected post hoc test when comparing 2 or more groups. A P value of less than 0.05 was considered statistically significant.

Study Approval. Ethical approval was obtained from the National Research Ethics Service Committee North East (14/NE/1076), United Kingdom. All animal experiments were performed under licenses granted from the Home Office (United Kingdom) in accordance with the guidelines and regulations for the care and use of laboratory animals outlined by the Animals (Scientific Procedures) Act 1986, and conducted according to protocols approved by the Animal Ethics Committee of Newcastle University and the Home Office, United Kingdom.

Subjects. We obtained DNA samples (blood/saliva) after obtaining informed consent from individuals with Joubert syndrome (with and without renal involvement) and Leber congenital amaurosis. Criteria for Joubert syndrome were based on the presence of cerebellar vermis aplasia/hypoplasia and/or molar tooth sign on brain MRI. Leber congenital amaurosis/retinal degeneration was diagnosed by an ophthalmologist. The diagnosis of renal disease was based on clinical course and renal ultrasound scan results.

Data Availability. We declare that all data supporting the findings of this study are available within the article, *SI Appendix.*
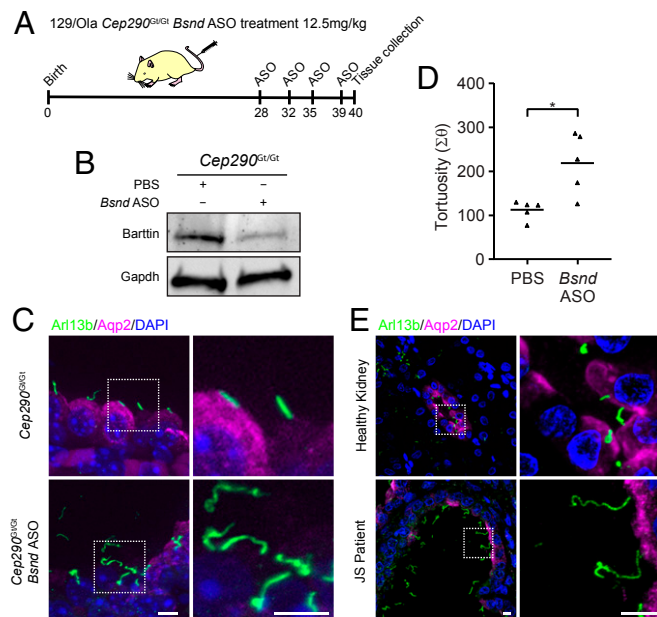
Fig. 3. Down-regulation of *Bsnd* in mouse recapitulates the human kidney phenotype. (*A*) Schematic showing the injection schedule of *Cep290*^Gt/Gt animals from a 129/Ola background. Mice were i.v. injected with an antisense oligonucleotide (ASO) targeted against the *Bsnd* gene, which codes for the CLC-type chloride channel accessory protein Barttin. (*B*) Western blot of murine kidney showing the reduction in Barttin protein level following knockdown with *Bsnd* ASO. (*C*) Immunofluorescence images of P21 mouse kidney from F2 *Cep290*^Gt/Gt animals on a 129/Ola background showing the expression of Arl13b (green) and Aqp2 (magenta) following injection of an ASO targeted against *Bsnd*. (Scale bars, 5 μm.) (*D*) Quantification of cilia tortuosity in *Cep290*^+/+ and *Cep290*^Gt/Gt animals (Student's t test, *$P < 0.05$). (*E*) Immunofluorescence images showing the expression of Arl13b (green) and Aqp2 (magenta) in a section of a kidney biopsy from a Joubert syndrome patient (NPH621: G/G at rs2500341; *SI Appendix,* Table S1) with end-stage renal disease secondary to mutations in *CEP290*. (Scale bars, 10 μm.)

1. H. J. S. Dawkins *et al.*; International Rare Diseases Research Consortium (IRDiRC), Progress in rare diseases research 2010–2016: An IRDiRC perspective. *Clin. Transl. Sci.* **11**, 11–20 (2018).
2. C. B. Bridges, The genetics of purple eye color in *Drosophila. J. Exp. Zool.* **28**, 265–305 (1919).
3. J. B. S. Haldane, The relative importance of principal and modifying genes in determining some human diseases. *J. Genet.* **41**, 149–157 (1941).
4. H. Corvol *et al.*, Genome-wide association meta-analysis identifies five modifier loci of lung disease severity in cystic fibrosis. *Nat. Commun.* **6**, 8382 (2015).
5. J. M. Lee *et al.*; Genetic Modifiers of Huntington's Disease (GeM-HD) Consortium, Identification of genetic factors that modify clinical onset of Huntington's disease. *Cell* **162**, 516–526 (2015).
6. S. M. Ware, M. G. Aygun, F. Hildebrandt, Spectrum of clinical diseases caused by disorders of primary cilia. *Proc. Am. Thorac. Soc.* **8**, 444–450 (2011).
7. M. Chaki *et al.*, Genotype-phenotype correlation in 440 patients with NPHP-related ciliopathies. *Kidney Int.* **80**, 1239–1245 (2011).
8. R. Shaheen *et al.*; Ciliopathy WorkingGroup, Characterizing the morbid genome of ciliopathies. *Genome Biol.* **17**, 242 (2016).
9. T. Suzuki *et al.*, Molecular genetic analysis of 30 families with Joubert syndrome. *Clin. Genet.* **90**, 526–535 (2016).
10. R. Bachmann-Gagescu *et al.*, Healthcare recommendations for Joubert syndrome. *Am. J. Med. Genet. A*, 10.1002/ajmg.a.61399 (11 November 2019).
11. J. A. Sayer *et al.*, The centrosomal protein nephrocystin-6 is mutated in Joubert syndrome and activates transcription factor ATF4. *Nat. Genet.* **38**, 674–681 (2006).
12. E. M. Valente *et al.*; International Joubert Syndrome Related Disorders Study Group, Mutations in CEP290, which encodes a centrosomal protein, cause pleiotropic forms of Joubert syndrome. *Nat. Genet.* **38**, 623–625 (2006).
13. A. I. den Hollander *et al.*, Mutations in the CEP290 (NPHP6) gene are a frequent cause of Leber congenital amaurosis. *Am. J. Hum. Genet.* **79**, 556–561 (2006).
14. L. Baala *et al.*, Pleiotropic effects of CEP290 (NPHP6) mutations extend to Meckel syndrome. *Am. J. Hum. Genet.* **81**, 170–179 (2007).
15. C. C. Leitch *et al.*, Hypomorphic mutations in syndromic encephalocele genes are associated with Bardet-Biedl syndrome. *Nat. Genet.* **40**, 443–448 (2008).
16. F. Coppieters, S. Lefever, B. P. Leroy, E. De Baere, CEP290, a gene with many faces: Mutation overview and presentation of CEP290base. *Hum. Mutat.* **31**, 1097–1108 (2010).
17. T. G. Drivas, A. P. Wojno, B. A. Tucker, E. M. Stone, J. Bennett, Basal exon skipping and genetic pleiotropy: A predictive model of disease pathogenesis. *Sci. Transl. Med.* **7**, 291ra97 (2015).
18. D. P. Norris, D. T. Grimes, Mouse models of ciliopathies: The state of the art. *Dis. Model. Mech.* **5**, 299–312 (2012).
19. A. M. Hynes *et al.*, Murine Joubert syndrome reveals Hedgehog signaling defects as a potential therapeutic target for nephronophthisis. *Proc. Natl. Acad. Sci. U.S.A.* **111**, 9893–9898 (2014).
20. P. Cela *et al.*, Ciliopathy protein Tmem107 plays multiple roles in craniofacial development. *J. Dent. Res.* **97**, 108–117 (2018).
21. R. R. Damerla *et al.*, Novel Jbts17 mutant mouse model of Joubert syndrome with cilia transition zone defects and cerebellar and other ciliopathy related anomalies. *Hum. Mol. Genet.* **24**, 3994–4005 (2015).
22. M. A. Lancaster *et al.*, Defective Wnt-dependent cerebellar midline fusion in a mouse model of Joubert syndrome. *Nat. Med.* **17**, 726–731 (2011).
23. R. A. Rachel *et al.*, CEP290 alleles in mice disrupt tissue-specific cilia biogenesis and recapitulate features of syndromic ciliopathies. *Hum. Mol. Genet.* **24**, 3775–3791 (2015).
24. M. Joubert, J. J. Eisenring, J. P. Robb, F. Andermann, Familial agenesis of the cerebellar vermis. A syndrome of episodic hyperpnea, abnormal eye movements, ataxia, and retardation. *Neurology* **19**, 813–825 (1969).
25. E. Boltshauser, W. Isler, Joubert syndrome: Episodic hyperpnea, abnormal eye movements, retardation and ataxia, associated with dysplasia of the cerebellar vermis. *Neuropadiatrie* **8**, 57–66 (1977).
26. S. Srivastava *et al.*, A human patient-derived cellular model of Joubert syndrome reveals ciliary defects which can be rescued with targeted therapies. *Hum. Mol. Genet.* **26**, 4657–4667 (2017).
27. H. Shimada *et al.*, In vitro modeling using ciliopathy-patient-derived cells reveals distinct cilia dysfunctions caused by CEP290 mutations. *Cell Rep.* **20**, 384–396 (2017).
28. S. A. Ramsbottom *et al.*, Targeted exon skipping of a *CEP290* mutation rescues Joubert syndrome phenotypes in vitro and in a murine model. *Proc. Natl. Acad. Sci. U.S.A.* **115**, 12489–12494 (2018).
29. R. Birkenhäger *et al.*, Mutation of BSND causes Bartter syndrome with sensorineural deafness and kidney failure. *Nat. Genet.* **29**, 310–314 (2001).
30. R. Estévez *et al.*, Barttin is a Cl– channel beta-subunit crucial for renal Cl– reabsorption and inner ear K+ secretion. *Nature* **414**, 558–561 (2001).
31. N. Jeck *et al.*, Hypokalemic salt-losing tubulopathy with chronic renal failure and sensorineural deafness. *Pediatrics* **108**, E5 (2001).
32. A. L. de Pablos *et al.*, Severe manifestation of Bartter syndrome type IV caused by a novel insertion mutation in the BSND gene. *Clin. Nephrol.* **81**, 363–368 (2014).
33. S. Nuovo *et al.*, Impaired urinary concentration ability is a sensitive predictor of renal disease progression in Joubert syndrome. *Nephrol. Dial. Transplant.*, 10.1093/ndt/gfy333 (6 November 2018).
34. L. A. Devlin, J. A. Sayer, Renal ciliopathies. *Curr. Opin. Genet. Dev.* **56**, 49–60 (2019).
35. H. Li, W. Yang, F. Mendes, M. D. Amaral, D. N. Sheppard, Impact of the cystic fibrosis mutation F508del-CFTR on renal cyst formation and growth. *Am. J. Physiol. Renal Physiol.* **303**, F1176–F1186 (2012).

www.manaraa.com